Single-Particle Motion in a Large-Orbit Gyrotron

HANS P. BLUEM, PETER E. LATHAM, WESLEY G. LAWSON, MEMBER, IEEE, AND CHARLES D. STRIFFLER, MEMBER, IEEE

Abstract—**The perturbation on the zeroth-order motion of individual particles in an axis-encircling, large-orbit gyrotron due to a constant-amplitude TE_{ln}^{0} electromagnetic (em) wave is studied analytically and numerically. Single-particle phenomena such as phase bunching and trapping are studied as a function of the frequency difference between the cyclotron motion and the em wave. Analytic solutions are developed for both trapped and untrapped particles and are compared with exact numerical results. The analytic solutions yield the percentage of trapped particles and an expression for the minimum em field necessary for trapping. It is shown that energy loss depends on first-order terms for trapped particles and on second-order terms for untrapped particles. A specific set of parameters is used to display the results.**

I. Introduction

THIS STUDY describes the interaction between an electromagnetic (em) wave and rotating electrons in a circular waveguide. The rotation of the electrons is produced by an externally applied magnetic field parallel to the waveguide. We confine our analysis to axis-encircling, concentric electrons, in which case the microwave tube is known as the large-orbit gyrotron (LOG) [1]–[3]. The LOG is a variation on the "conventional," or small-orbit, gyrotron [4]–[6].

The instability that drives both the LOG and the small-orbit gyrotron arises from the negative mass effect, which causes electrons to phase bunch in the em wave. When the wave frequency ω differs from the frequency associated with beam bunching, $l\omega_c + k_z v_z$, there is a net energy exchange between the em wave and the bunched electrons. In our notation, l is the azimuthal harmonic mode number of the em wave, $\omega_c = eB_0/\gamma m_0$ is the electron cyclotron frequency, k_z is the axial wavenumber, and v_z is the parallel velocity of the electrons.

The degree of bunching is a function of both the field amplitude and the size of the frequency mismatch, $\omega - l\omega_c - k_z v_z$. There is always some tendency for the particles to bunch, but the formation of tight bunches occurs only for a narrow range of parameters. For small enough frequency mismatch or large enough wave amplitude, the particles become trapped. When trapping occurs, the particles no longer rotate at the cyclotron frequency, but become synchronized with the wave. This effect, which is accompanied by a large exchange of wave and particle energy, is essential for high-efficiency operation.

The large-orbit gyrotron can operate as either an oscillator or an amplifier. The mode considered here is conceptually that of an amplifier, in which there is linear spatial growth near the front of the tube. Farther downstream, however, saturation occurs, yielding a steady-state configuration in which the loss in beam kinetic energy is balanced by the production of em radiation. Thus, in the saturated region, the particles see an approximately constant-amplitude wave. It is this region that is of interest to us; to analyze it we adopt the single-particle formalism. We assume that the particle distribution is uniform in the saturated region. This is analogous to the "sudden" approximation employed by Thode and Sudan [7], [8] in their analysis of the two-stream instability. Its validity rests on the observation that the waves go from the linear regime to the nonlinear regime in only a few e-foldings. Thus, unless the growth rate is exceptionally slow, the particles are not significantly perturbed when they enter the saturated region. While a more accurate treatment would take such perturbations into account, they are not important to the qualitative picture we seek to develop here.

Even though the single-particle formalism suffers from the inherent drawback that it cannot predict the self-consistent amplitude and frequency mismatch, its advantage lies in its ability to isolate the important physical effects associated with the nonlinear particle trajectories. In particular, we are able to derive approximate analytical expressions for both trapped and untrapped particles and study a broad range of em field parameters.

We assume that the beam density is low enough that the particles interact with a single empty waveguide mode of constant amplitude and frequency [3]. Within this context, we study bunch formation as well as the effect of bunching on energy exchange. The study of the particle motion is done both numerically and analytically. However, we emphasize the development of the analytic solutions which describe the particle motion in both the linear and nonlinear regimes.

In the gyrotron literature, only a few papers deal with the actual particle orbits and the relationship between single-particle motion and energy exchange. Sprangle and Drobot [9] consider a configuration composed of a gyrating beam interacting with a TE_{0n} rectangular mode be-

Manuscript received February 12, 1987; revised June 29, 1987. This work was supported by the Air Force Office of Scientific Research

The authors are with the Electrical Engineering Department and the Laboratory for Plasma and Fusion Energy Studies, University of Maryland, College Park, MD 20742.

IEEE Log Number 8716594.

tween two parallel conducting plates. They discuss the relationship between trapping and the electric field amplitude. Vomvoridis [10] also examines a small-orbit gyrotron and studies the effects of frequency mismatch, initial beam energy, and interaction length on energy loss. More importantly, he studies the relative importance of trapped and untrapped particles. Vitello *et al.* [11] study particle motion in a large-orbit gyrotron. They solve the single-particle equations of motion for a system with a cylindrical cavity. The analytic solutions they obtain are valid for untrapped particles only. They also present a numerical study, calculating efficiencies over a wide range of parameters.

In Section II a detailed description of the problem is given. Analytic solutions are presented in Section III. Two different solutions are developed, each pertaining to a different class of particles. In Section IV, the analytic solutions are compared to the numerical solutions, and some general results are presented for a specific set of system parameters. A summary is presented in Section V.

II. Model and Basic Formalism

A schematic of the large-orbit gyrotron system is given in Fig. 1. This figure shows the zeroth-order particle motion and the perturbing em wave parameters. The zeroth-order motion of an axis-encircling, concentric electron cyclotron orbit is given by

$$\begin{aligned} r(t) &= r_0 \\ \phi(t) &= \phi_0(t) = \phi_{00} + \omega_c t \\ z(t) &= z_0(t) = z_{00} + v_{z_0} t \\ v_r(t) &= v_{r_0} = 0 \\ v_\phi(t) &= v_{\phi_0} = \beta_{\phi_0} c = r_0 \omega_c \\ v_z(t) &= v_{z_0} = \beta_{z_0} c \\ \gamma(t) &= \gamma_0 = \left(1 - \beta_{\phi_0}^2 - \beta_{z_0}^2\right)^{-1/2}. \end{aligned} \tag{1}$$

The particle's cyclotron radius is r_0, its perpendicular velocity is v_{ϕ_0}, and its parallel velocity is v_{z_0}. The em wave is defined by its amplitude E_p, its mode numbers l and n, and its axial wavenumber k_z. The waveguide radius is given by r_w. A cylindrical coordinate system is used throughout this paper.

The single-particle motion is determined by the relativistic Lorentz force equation

$$\frac{d}{dt}(m\gamma\vec{v}) = -e\left[\vec{E} + \vec{v}\times\left(\vec{B} + \vec{B}_0\right)\right] \tag{2}$$

from which it follows that

$$\frac{d\gamma}{dt} = \frac{-e}{mc^2}\left(\vec{v}\cdot\vec{E}\right) \tag{3}$$

where $\vec{v}$ is the electron velocity, $\vec{E}$ and $\vec{B}$ are the electric and magnetic fields of the em wave, and $\vec{B}_0 = B_0\hat{z}$. In general, the electric and magnetic fields contain all components: $\vec{E} = (E_r, E_\phi, E_z)$ and $\vec{B} = (B_r, B_\phi, B_z)$. For the purposes of this paper, we consider only TE waveguide modes ($E_z = 0$). We concentrate on an example that has nearly grazing intersection between the dispersion curves, and we neglect the TM modes, since their linear growth rate goes to zero at grazing intersection [3]. In the gyrotron interaction, the azimuthal component of the electric field E_ϕ exerts the dominant em force. This field component is given by

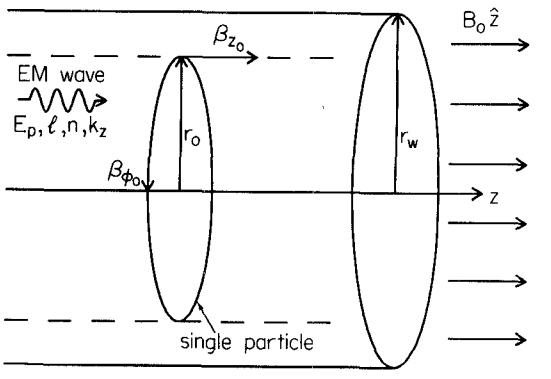

Fig. 1. Large-orbit gyrotron system showing single-particle zeroth-order motion and the em wave.

$$E_\phi = E_p J_l'(\alpha_{ln} r)\sin(\omega t - k_z z - l\phi) \tag{4}$$

where J_l' represents the derivative of the ordinary Bessel function of order l, $\alpha_{ln} = p'_{ln}/r_w$, where p'_{ln} is the nth root of J_l', and k_z and ω are related by the dispersion equation

$$\omega = c\left(k_z^2 + \alpha_{ln}^2\right)^{1/2}. \tag{5}$$

To understand the effects of the em wave on the LOG particles, we linearize the Lorentz force equation, treating the em fields as first-order quantities. Linearizing the particles' position about the zeroth-order locations as given in (1) [$r(t) = r_0 + r_1(t)$, $\phi(t) = \phi_0(t) + \phi_1(t)$, $z(t) = z_0(t) + z_1(t)$], we obtain from (2) the set of equations

$$\ddot{r}_1 - r_0\omega_c\dot{\phi}_1 - r_0\omega_c^2\frac{\gamma_1}{\gamma_0} = -\frac{e}{m\gamma_0}\left[E_{r_1} + r_0\omega_c B_{z_1} - v_{z_0}B_{\phi_1}\right] \tag{6}$$

$$r_0\ddot{\phi}_1 + \omega_c\dot{r}_1 + r_0\omega_c\frac{\dot{\gamma}_1}{\gamma_0} = -\frac{e}{m\gamma_0}\left[E_{\phi_1} + v_{z_0}B_{r_1}\right] \tag{7}$$

$$\ddot{z}_1 + v_{z_0}\frac{\dot{\gamma}_1}{\gamma_0} = -\frac{e}{m\gamma_0}\left[E_{z_1} - r_0\omega_c B_{r_1}\right] \tag{8}$$

where $\dot{\gamma}_1$ is given by

$$\frac{\dot{\gamma}_1}{\gamma_0} = -\frac{e}{m\gamma_0 c^2}\left[r_0\omega_c E_{\phi_1} + v_{z_0}E_{z_1}\right]. \tag{9}$$

The azimuthal component of the electric field (4) evaluated

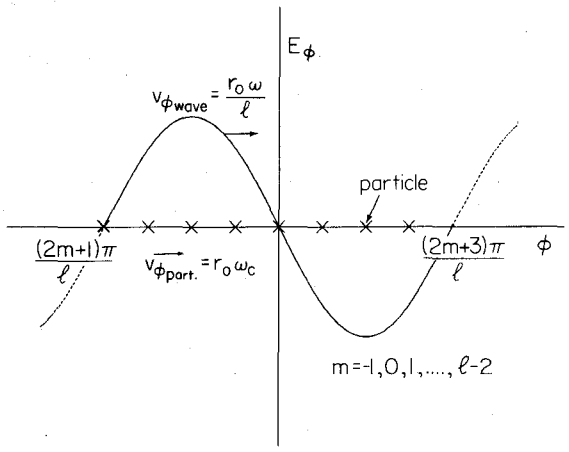

Fig. 2. The relationship of a group of particles with respect to the azimuthal electric field E_ϕ.

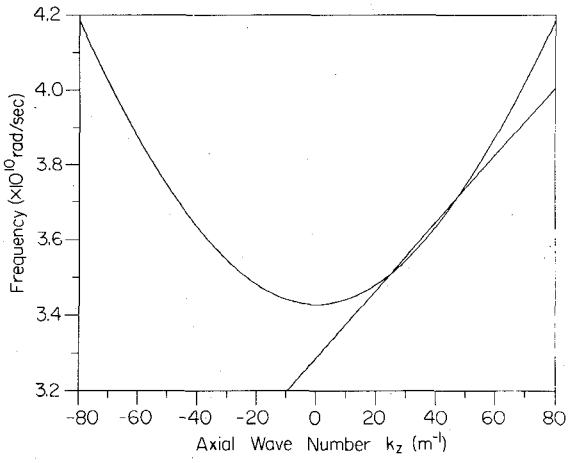

Fig. 3. Dispersion curve in the laboratory frame. Parameters given in Table I.

at the particle position becomes

$$E_{\phi_1} = E_p J_l'(\alpha_{ln} r_0) \cdot \sin\left[\omega_D t - k_z z_{00} - l\phi_{00} - k_z z_1(t) - l\phi_1(t)\right] \quad (10)$$

where $\omega_D \equiv \omega - l\omega_c - k_z v_{z_0}$ is the difference between the em frequency ω and the particle frequency $l\omega_c + k_z v_{z_0}$. To obtain a solution to (6)–(8), a number of parameters must be specified. The parameters associated with the particle are r_0, ϕ_{00}, z_{00}, v_{ϕ_0}, and v_{z_0}; those associated with the wave are n, l, k_z, E_p, and r_w. Of these parameters, only three need to be varied to assess the effects of the em wave on the particle motion: the initial phase of the particle in the wave, ϕ_{00}, the axial wavenumber, k_z, and the amplitude of the wave, E_p.

Taking advantage of the azimuthal periodicity of the em wave, the range of ϕ_{00} can be limited to one wave period, $2\pi/l$ radians. For a set of particles uniformly distributed in one wave period, as displayed in Fig. 2, we can vary either k_z or the wave amplitude to observe the effects of bunching and trapping on each particle. Fig. 2 also shows

TABLE I
PARAMETERS FOR THE CASE STUDY: LABORATORY FRAME

	Parameter	Value(s)
Wave	k_z	36 to 74 m^{-1}
	E_p	1.05×10^5 to 1.13×10^7 V/m
	ℓ	7
	n	1
	Mode	TE
	r_w	0.075 m
Particle	r_o	0.06 m
	ϕ_{oo}	$-\pi/\ell$ to $+\pi/\ell$ radians
	z_o	0.00 m
	β_{r_o}	0.0
	β_{ϕ_o}	0.941 (γ = 6.29)
	β_{z_o}	0.3

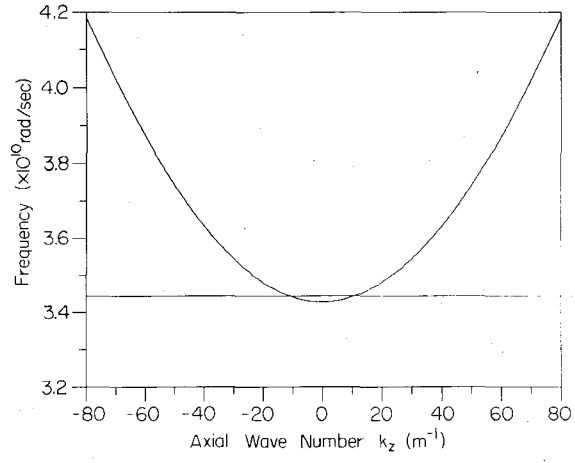

Fig. 4. Dispersion curve transformed to the beam frame. Parameters given in Table II.

the two relevant azimuthal velocities: for the wave, $v_{\phi_{wave}} = r_0\omega/l$, and for the particles, $v_{\phi_{part.}} = v_{\phi_0} = r_0\omega_c$. We see that $\omega - l\omega_c$ is proportional to the difference in these velocities. When the longitudinal variation in the wave is included, a factor $k_z v_{z_0}$ is introduced, leaving $\omega - l\omega_c - k_z v_{z_0}$ as the difference in frequencies in the laboratory frame. A typical plot of the waveguide dispersion curve and the beam line is shown in Fig. 3, where the parameters of Table I are used. At resonance, $\omega = l\omega_c + k_z v_{z_0}$; this point is indicated by the crossing of the beam line and the waveguide dispersion curve.

To simplify the analysis, we Lorentz transform from the laboratory frame (finite β_{z_0}) to the beam frame ($\beta_{z_0}' = 0$). The equivalent beam frame dispersion curve is shown in Fig. 4. Again, specific values are plotted, this time using Table II parameters. When the axial velocity of the particles is small ($\beta_{z_0} \lesssim 0.3$), the values of the parameters in

TABLE II
PARAMETERS FOR THE CASE STUDY: BEAM FRAME

	Parameter	Value(s)
Wave	k_z'	0.0 to 35.0 m^{-1}
	E_p'	10^5 to 10^7 V/m
	ℓ'	7
	n'	1
	Mode	TE
	r_w'	0.075 m
Particle	r_o'	0.06 m
	ϕ_{oo}'	$-\pi/\ell$ to $+\pi/\ell$ radians
	z_o'	0.00 m
	β_{r_o}'	0.0
	β_{ϕ_o}'	0.986 ($\gamma = 6$)
	β_{z_o}'	0.0

the beam frame are not significantly different from the actual values in the laboratory frame (compare Tables I and II). For the remainder of this paper all work is done in the beam frame and for clarity, the primes are dropped.

III. Analytic Solutions

The solution to (6)–(8) depends crucially on whether or not the particle is trapped. For untrapped particles, the dominant motion is given by the cyclotron orbits in the uniform magnetic field, and the em fields produce small oscillations around the unperturbed orbits; these oscillations are easily handled using standard techniques. For trapped particles, on the other hand, the final particle motion is radically different from the original cyclotron orbits. First, the particles become synchronized with the em wave, so their average rotation frequency shifts from ω_c to ω. Second, because the particles exhibit large excursions from the minimum of the effective potential associated with E_ϕ, the oscillations around the average motion are highly nonlinear. These two effects combine to make the trapped particle analysis considerably more difficult than that of the untrapped particles. However, we are able to derive approximate analytic solutions for both types of orbits. We consider untrapped particles first, as the analysis is simpler.

A. Untrapped Solution

The condition that leads to untrapped solutions is that $\phi_1(t)$ and $z_1(t)$ in (10) remain negligible for all time. Mathematically this condition is $l\phi_1(t) \ll 2\pi$ and $k_z z_1(t) \ll 2\pi$. This is the assumption used by Vitello *et al.* in their derivation. Working in the beam frame ($v_{z_0} = 0$), ignoring the contributions from E_{r_1}, B_{r_1}, B_{z_1}, and B_{ϕ_1}, and assuming that the above inequalities are satisfied, (6)–(8) become

$$\ddot{r}_1 - r_0\omega_c\dot{\phi}_1 = \frac{e}{m\gamma_0}\beta_{\phi_0}^2\frac{\omega_c}{\omega_D}E_p J_l'(\alpha_{ln}r_0) \cdot\left[\cos(\omega_D t - l\phi_{00}) - \cos(l\phi_{00})\right] \tag{11}$$

$$r_0\ddot{\phi}_1 + \omega_c\dot{r}_1 = -\frac{e}{m\gamma_0}\left(1-\beta_{\phi_0}^2\right)E_p J_l'(\alpha_{ln}r_0)\sin(\omega_D t - l\phi_{00}) \tag{12}$$

$$\ddot{z}_1 = 0 \tag{13}$$

where (9) has been used to eliminate $\dot{\gamma}_1$ and γ_1 [$\gamma_1(0) = 0$], and z_{00} has been set to zero. The terms proportional to $\beta_{\phi_0}^2$, which arise from the time dependence of γ_1, give rise to the negative mass effect. Using standard techniques, these equations result in the following first-order particle motion:

$$r_1(t) = -\frac{e}{m\gamma_0}\frac{E_p}{\omega_c^2-\omega_D^2}J_l'(\alpha_{ln}r_0) \cdot\left[\sin l\phi_{00}\sin\omega_c t + \frac{\omega_D}{\omega_c}\cos l\phi_{00}\cos\omega_c t - \frac{\omega_c}{\omega_D}\cos(\omega_D t - l\phi_{00}) + \frac{\omega_c^2-\omega_D^2}{\omega_c\omega_D}\cos l\phi_{00}\right] \tag{14}$$

$$\phi_1(t) = \frac{e}{m\gamma_0}\frac{E_p}{\omega_c^2-\omega_D^2}\frac{J_l'(\alpha_{ln}r_0)}{r_0} \cdot\left\{\left[\cos\omega_D t - \cos\omega_c t\right]\sin l\phi_{00} + \left[\frac{\omega_D}{\omega_c}\sin\omega_c t - \sin\omega_D t\right]\cos l\phi_{00} + \beta_{\phi_0}^2\left(\frac{\omega_c^2-\omega_D^2}{\omega_D^2}\right) \times\left[-(1-\cos\omega_D t)\sin l\phi_{00} + (\omega_D t - \sin\omega_D t)\cos l\phi_{00}\right]\right\} \tag{15}$$

$$z_1(t) = 0 \tag{16}$$

$$\gamma_1(t) = \frac{e}{m\gamma_0}\frac{\gamma_0\beta_{\phi_0}}{c}\frac{E_p}{\omega_D}J_l'(\alpha_{ln}r_0) \cdot\left[\cos(\omega_D t - l\phi_{00}) - \cos l\phi_{00}\right]. \tag{17}$$

These solutions exhibit oscillations at two distinct frequencies, ω_c and ω_D. Oscillations at ω_c are a residual effect of the cyclotron motion and are not especially important. Oscillations at ω_D, on the other hand, represent the main effect of the perturbing em wave; they arise from the beating between the cyclotron motion and the wave. Note that the amplitude of the oscillations in ϕ_1 is proportional to $1/\omega_D^2$; this is typical of a near-resonant interaction.

In addition to the two frequencies ω_c and ω_D, there is also a term linear in t in the expression for ϕ_1. This term arises because particles with different initial phase have

different total energy, and thus different values of ω_c; it is essentially a correction to the relativistic cyclotron frequency. The smallness of the linear term indicates that the particles do indeed remain untrapped. For trapped particles, there is a much larger linear term that is proportional to the difference frequency ω_D. We will see this explicitly when we discuss the trapped solutions below.

An important feature of these solutions is that the first-order energy $mc^2\gamma_1$, averaged over initial phase ϕ_{00}, is zero. Consequently, whenever the untrapped solutions are valid, the net energy exchange is at least second order. This is typical of the interaction of an unbunched beam with a nonresonant wave.

The range of validity of the untrapped solution is found by combining the condition $l\phi_1 \ll 2\pi$ with (15). The resulting inequality may be written

$$\frac{E_p}{cB_0} \ll \frac{2\pi}{l}\frac{1}{J_l'(\alpha_{ln}r_0)}\frac{1}{\beta_{\phi_0}}\left(\frac{\omega_D}{\omega_c}\right)^2 \tag{18}$$

for $t \gtrsim 1/\omega_D$. No matter how small the electric field, this condition is violated as $\omega_D \to 0$.

We have derived solutions analogous to (14)–(17) that include all the TE field components, and we found that the contribution from E_{ϕ_1} dominates all aspects of the particle motion for the cases considered. This is supported by numerically solving the full system of equations, although the E_{ϕ_1}-only results begin to show departures from the true solution for particles that approach the trapped–untrapped border.

B. Trapped Solution

For a trapped particle, the zeroth-order motion of the phase angle is no longer given by $\phi(t) = \phi_{00} + \omega_c t$. Instead, the particle becomes synchronized with the wave, and $l\phi(t) \sim \omega t$. To model this behavior, we let

$$\phi_1(t) = \frac{a_0}{2} + a_1\cos(\omega_B t - \theta) + \frac{\omega_D}{l}t + \phi_2(t) \tag{19}$$

where again $\phi(t) = \phi_{00} + \omega_c t + \phi_1(t)$. The term $\omega_D t/l$ ensures that $l\phi(t)$ is proportional to ωt. Consistent with our physical picture of a particle trapped in an effective potential, we include the term $a_1\cos(\omega_B t - \theta)$ to model the oscillations about the bottom of the well; the term $a_0/2$ is included so that the particles oscillate around the potential minimum. The function $\phi_2(t)$ is assumed small. We expect this form of the solution to describe particle motion near the bottom of the potential, where there is a well-defined bounce frequency. Although valid when the bounce oscillations are small, this solution breaks down near the trapping boundary.

To proceed, we insert (19) into (6)–(8) and solve for the quantities a_0, a_1, ω_B, and θ. As with the untrapped solution, we assume that r_1, $k_z z_1$, and γ_1 are small. After some algebra, we find that

$$\begin{aligned}\ddot{r}_1 - \omega_c r_0\dot{\phi}_2 = {} & \frac{e}{m\gamma_0}\omega_c\beta_{\phi_0}^2 E_p J_l'(\alpha_{ln}r_0) \\ & \cdot\int_0^t \sin\left[l\phi_{00} + \frac{la_0}{2} \right. \\ & \left. + la_1\cos(\omega_B t' - \theta)\right]dt' \\ & + \omega_c r_0\left[\frac{\omega_D}{l} - \omega_B a_1\sin(\omega_B t - \theta)\right] \end{aligned} \tag{20}$$

$$\begin{aligned} r_0\ddot{\phi}_2 + \omega_c\dot{r}_1 = {} & \frac{e}{m\gamma_0}\left(1-\beta_{\phi_0}^2\right)E_p J_l'(\alpha_{ln}r_0)\sin \\ & \cdot\left[l\phi_{00} + \frac{la_0}{2} + la_1\cos(\omega_B t - \theta)\right] \\ & + r_0\omega_B^2 a_1\cos(\omega_B t - \theta) \end{aligned} \tag{21}$$

$$\ddot{z}_1 = 0. \tag{22}$$

Again, we have included only E_ϕ for a TE waveguide mode, and we have assumed that $\phi_2(t)$ is of the same order as $r_1(t)$ and $z_1(t)$.

To solve these equations, the sine term on the right-hand side must be simplified. To ensure that the particle oscillates around the zero of E_ϕ, we require that

$$\frac{la_0}{2} + l\phi_{00} = 0, 2\pi, 4\pi, \cdots. \tag{23}$$

Using this result and the periodicity of the sine function, we are left with terms of the form $\sin[la_1\cos(\omega_B t - \theta)]$. These can be expanded using [12]:

$$\sin(z\cos\xi) = 2\sum_{k=0}^{\infty}(-1)^k J_{2k+1}(z)\cos[(2k+1)\xi] \tag{24}$$

leaving only $\cos(\omega_B t - \theta)$ terms on the right-hand side. The remaining equations can be solved using Laplace transforms and the appropriate initial conditions on the position and velocity, resulting in

$$\begin{aligned} r_1(t) = {} & \frac{2e}{m\gamma_0}\frac{E_p}{\omega_c\omega_B}J_l'(\alpha_{ln}r_0)\sum_{k=0}^{\infty}(-1)^k\frac{J_{2k+1}(la_1)}{2k+1} \\ & \times\left\{\frac{\omega_c^2}{\omega_c^2 - [(2k+1)\omega_B]^2}\left[\sin[(2k+1)(\omega_B t - \theta)]\right.\right. \\ & - \frac{(2k+1)^2\omega_B^2}{\omega_c^2}\cos\omega_c t\sin[(2k+1)\theta] + \frac{(2k+1)\omega_B}{\omega_c} \\ & \left.\left.\times\sin\omega_c t\cos[(2k+1)\theta]\right] + \sin[(2k+1)\theta]\right\} \end{aligned} \tag{25}$$

$$\phi_2(t) = \frac{2e}{m\gamma_0}\frac{E_p}{\omega_B^2}\frac{J_l'(\alpha_{ln}r_0)}{r_0}\sum_{k=0}^{\infty}(-1)^k J_{2k+1}(la_1)$$

$$\cdot\left\{\frac{\omega_B^2}{\omega_c^2-[(2k+1)\omega_B]^2}\left[\left(1-\beta_{\phi_0}^2+\frac{\omega_c^2}{\omega_B^2}\frac{\beta_{\phi_0}^2}{(2k+1)^2}\right)\right.\right.$$

$$\cdot\cos[(2k+1)(\omega_B t-\theta)]-\cos\omega_c t\cos[(2k+1)\theta]$$

$$\left.-\frac{(2k+1)\omega_B}{\omega_c}\sin\omega_c t\sin[(2k+1)\theta]\right]$$

$$-\frac{\beta_{\phi_0}^2}{(2k+1)^2}[\cos[(2k+1)\theta]+(2k+1)\omega_B t$$

$$\left.\cdot\sin[(2k+1)\theta]]\right\}-\frac{\omega_D t}{l}-\frac{a_0}{2}-a_1\cos(\omega_B t-\theta) \quad (26)$$

$$z_1(t)=0 \quad (27)$$

and

$$\gamma_1(t) = \frac{2e}{m\gamma_0}\frac{\gamma_0\beta_{\phi_0}}{c}\frac{E_p}{\omega_B}J_l'(\alpha_{ln}r_0)\sum_{k=0}^{\infty}(-1)^k\frac{J_{2k+1}(la_1)}{2k+1}$$

$$\times\{\sin[(2k+1)(\omega_B t-\theta)]+\sin[(2k+1)\theta]\}. \quad (28)$$

From (18) and (26) we can determine the expression for ϕ_1. To obtain the values of a_0, a_1, ω_B, and θ, a direct comparison is made between the approximation for ϕ_1 (from (18)) and the solution for ϕ_1 (from (26)). In addition to the condition given in (23), comparing constant terms yields

$$\frac{a_0}{2} = -\frac{2e}{m\gamma_0}\beta_{\phi_0}^2\frac{E_p}{\omega_B^2}\frac{J_l'(\alpha_{ln}r_0)}{r_0}$$

$$\cdot\sum_{k=0}^{\infty}(-1)^k\frac{J_{2k+1}(la_1)}{(2k+1)^2}\cos[(2k+1)\theta]. \quad (29)$$

Terms linear in t give

$$\frac{\omega_D}{l} = -\frac{2e}{m\gamma_0}\beta_{\phi_0}^2\frac{E_p}{\omega_B}\frac{J_l'(\alpha_{ln}r_0)}{r_0}$$

$$\cdot\sum_{k=0}^{\infty}(-1)^k\frac{J_{2k+1}(la_1)}{(2k+1)}\sin[(2k+1)\theta]. \quad (30)$$

Finally, terms with $\cos(\omega_B t-\theta)$ give

$$a_1 = \frac{2e}{m\gamma_0}\frac{E_p}{\omega_c^2-\omega_B^2}\frac{J_l'(\alpha_{ln}r_0)}{r_0}J_1(la_1)\left(1+\frac{\omega_c^2-\omega_B^2}{\omega_B^2}\beta_{\phi_0}^2\right). \quad (31)$$

The remaining terms comprise ϕ_2. While these expressions appear complicated, in practice only the first one or two terms in the Bessel function expansion are needed. This results in a tractable set of equations for a_0, a_1, ω_B, and θ.

IV. Comparison of Solutions and Results

To display the results, we use the parameters given in Table II. These values, which are the transformed parameters of Table I, model the Rotating Beam Facility (RBF) at the University of Maryland [2]. The mode number is chosen to be $l=7$; this is the first harmonic that has a resonant intersection. The laboratory and beam frame dispersion curves are plotted in Figs. 3 and 4, respectively.

A. Comparison of Analytic and Exact Numerical Solutions

1) Untrapped: A comparison of the analytic (15) and the exact numerical solutions of the full set of Lorentz equations for an untrapped particle is shown in Fig. 5. The numerical solutions are obtained by integrating the relativistic single-particle equations of motion using all fields of the TE mode. We have plotted $l[\phi(t)-\omega_c(t)]=l[\phi_{00}+\phi_1(t)]$ versus time for a single particle using the parameters given in Table II, with $E_p=10^5$ V/m and $k_z=27$ m^{-1}. For these parameters the cyclotron period is 1.3 ns. We have chosen a wave centered at zero radians with a positive peak at $-\pi/14$ rad. Thus, the wave period extends from $-\pi/7$ to $\pi/7$ rad.

For the values chosen, all of the particles in an azimuthal wave period are untrapped. The particle shown in Fig. 5 is at the positive peak of the wave, $l\phi_{00}=-90°$. For this particle, $l\phi_1$ varies by at most 7°, satisfying the assumption used to obtain the untrapped solutions: $l\phi_1 \ll 360°$. Physically, the particle and the phase velocity differ sufficiently that the particle velocity is perturbed only slightly; the distance from resonance is approximately 0.75×10^9 rad/s, which for this relative low field strength is quite large. Note that there is a slight increase in phase due to the term linear in time in (15).

2) Trapped: The comparison of the trapped solutions (19), (26), and (29)–(31) with the exact numerical solution is shown in Fig. 6. We have plotted $l[\phi(t)-\omega t]$ versus time for a single particle using the parameters given in Table II, with $E_p=10^6$ V/m and $k_z=27$ m^{-1}. Since the particle is trapped, we have plotted our results in the wave frame. Again, we have chosen a wave centered at zero radians with a maximum at $-\pi/14$ rad, and we have chosen a particle at the positive peak of the wave, $l\phi_{00}=-90°$. This particle is close to the trapped–untrapped border, which occurs at $l\phi_{00}\approx-101.2°$, and its trajectory extends down to the edge of the wave ($-180°$). The figure

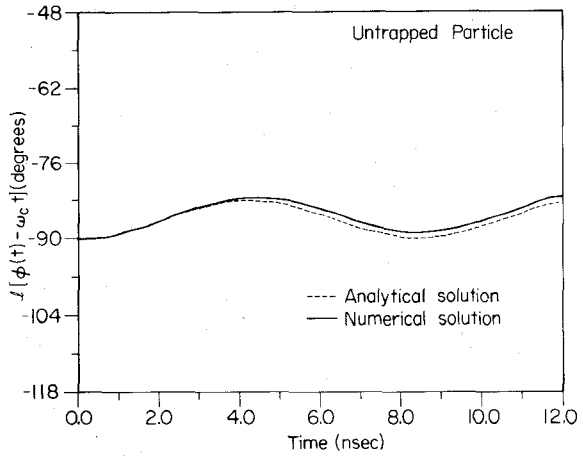

Fig. 5. Comparison between the analytic solution and the numerical solution for an untrapped particle.

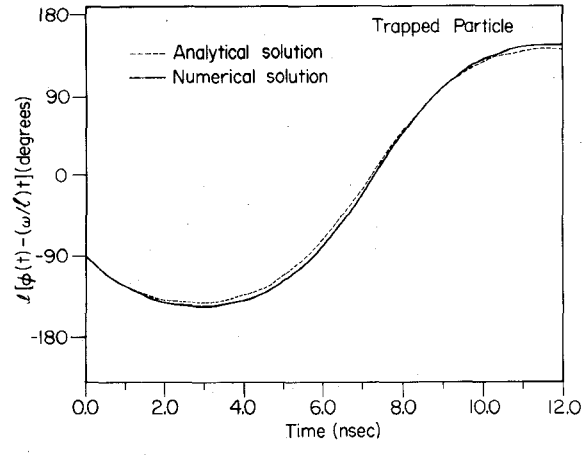

Fig. 6. Comparison between the analytic solution and the numerical solution for a trapped particle.

again shows only the azimuthal motion. Although not shown in this figure, the trapped solutions become worse as the trapping border is approached, but even very close to the border the approximate analytic solutions are reasonably accurate. However, for particles between the central zero of the wave and its maximum, the agreement between the two solutions is better than shown. Between the trapped solutions' region of validity and the region where the untrapped solutions are accurate, an area exists where we do not have a good analytic solution. Even though these particles are untrapped, they are close enough to resonance that (18) is violated; consequently, they develop a significant phase shift that cannot be taken into account by the untrapped analysis. In the next section we show that this region is relatively unimportant as far as net energy loss is concerned.

B. Results and Discussion

To evaluate the parameters associated with trapped particle orbits, we first choose a_1 in (29)–(31). Using a_1 we can find ω_B from (31). Then (30) and (29) are solved for θ and then a_0. Finally, a_0 gives us the initial azimuthal position of the particle, ϕ_{00}. Since we must pick a_1 first for the trapped solutions and then determine ϕ_{00}, it is difficult to choose a particular particle in the wave as is done for the numerical solutions. However, an advantage to this approach is that the solutions produce the range in ϕ_{00} for which particles are trapped. The upper limit on a_1 for any set of parameters is π/l. The lower limit can be found by setting $\theta = \pi/2$; this ensures that the particle starts at the zero of E_ϕ. With $\theta = \pi/2$, (30) and (31) can be solved simultaneously for $a_{1_{\min}}$. The condition that a_1 must lie between $a_{1_{\min}}$ and π/l for any trapped particle can be used to obtain the limits for ϕ_{00}. In addition, the upper limit ($a_1 = \pi/l$) gives the particles on the trapped–untrapped border, and the percentage of particles trapped can easily be found.

With the knowledge of the limits on a_1, we can calculate the average energy loss or gain, $\bar{\gamma}_1$, due to the trapped particles. This is given by

$$\bar{\gamma}_1 = \frac{\int_{a_{1_{\min}}}^{\pi/l} \gamma_1 \, da_1}{(\pi/l) - a_{1_{\min}}}. \tag{32}$$

Note that $\bar{\gamma}_1$ is nonzero for the trapped solutions. This expression, with the denominator replaced by π/l to represent all the particles, trapped and untrapped, is used in Fig. 9 to determine the average energy loss per particle.

Another quantity which can be obtained from our solutions is the minimum electric field for which trapping occurs (for a given set of parameters). The first particle to be trapped is the one in the central zero of the wave period, so $\phi_{00} = 0$; consequently, $a_0 = 0$ and $\theta = \pi/2$. For the minimum field, this particle is on the trapped–untrapped border, so we also have $a_1 = \pi/l$. Applying these conditions to (30) and (31) and making the simplifying assumption that $\omega_B \ll \omega_c$, we find that

$$\frac{\omega_D/l}{(E_{p_{\min}})^{1/2}} = \left(\frac{\pi}{l}\right)^{1/2}\left[\frac{2\omega_c J_l'(\alpha_{ln} r_0)}{B_0 r_0}\right]^{1/2} \cdot \frac{\beta_{\phi_0}}{J_1^{1/2}(\pi)} \sum_{k=0}^{\infty} (-1)^k \frac{J_{2k+1}(\pi)}{2k+1}. \tag{33}$$

This gives a relationship between the distance from resonance of the particles and the smallest E field ($E_{p_{\min}}$) necessary for trapping.

Besides the quantitative information provided by the solutions, considerable qualitative information about the particle motion can be obtained. First, the effect of the distance from resonance on the percentage of trapped particles can be deduced from (29)–(31). Since the value of a_1 remains constant for the border particle, we see from (31) that ω_B remains constant. Thus, if ω_D is increased, (30) implies that there must be a corresponding increase in θ (note that θ lies between zero and $\pi/2$); then, from (29), we see that a_0 must decrease. Consequently, for the border particle ϕ_{00} shifts toward the center of the wave period as ω_D increases, implying that the number of trapped particles decreases as the distance from resonance increases.

To understand the scaling with E_p, we again make the physically reasonable assumption that the bounce frequency is much less than the cyclotron frequency; $\omega_B \ll \omega_c$. Then, because a_1 is bounded, (31) yields $\omega_B \propto \sqrt{E_p}$. This dependence is typical of particle oscillations in the potential well formed by an electric field of strength E_p.

The effect of changing E_p or ω_D on an individual particle can be seen easily only for the particle with $a_0 = 0$, i.e., the one in the central zero. Using the condition that $la_1 \leq \pi/2$, so that $J_3(la_1) \ll J_1(la_1)$, and again assuming that $\omega_B \ll \omega_c$, we find that

$$\omega_B = \frac{2l\omega_c\beta_{\phi_0}^2 J_1(la_{1_{\min}})E_p J_l'(\alpha_{ln}r_0)}{\omega_D B_0 r_0} = \frac{\omega_D}{a_{1_{\min}} l} \tag{34}$$

and

$$a_{1_{\min}} J_1(la_{1_{\min}}) = \frac{\omega_D^2 B_0 r_0}{2l^2\omega_c\beta_{\phi_0}^2 E_p J_l'(\alpha_{ln}r_0)}. \tag{35}$$

Consistent with our physical intuition, (34) and (35) indicate that a_1 decreases and ω_B increases as E_p/ω_D^2 increases.

C. Graphical Results and Discussion

In this section we present the net energy loss or gain as a function of time, bunching in the azimuthal electric field, and trapping versus distance from resonance. Fig. 7 shows the percentage of particles trapped as a function of distance from resonance for both the analytic and the numerical solution; this figure uses the parameters of Table II with $E_p = 10^6$ V/m. While there is a good correlation between the two solutions in most of the region, near resonance the discrepancy becomes significant. However, since the region of maximum energy loss occurs away from resonance, this problem does not limit the solutions' usefulness in evaluating other important effects. In addition, we find that in the region close to resonance the particles responsible for the dominant portion of energy exchange are not near the trapping border. Thus, the error in the number of trapped particles does not have a large effect on energy loss or gain.

It turns out that the dominant contribution to energy loss comes from the trapped particles. We alluded to this result earlier when we showed that the first-order energy loss is zero for untrapped particles, while it is nonzero for trapped particles. A set of graphs to illustrate this point is given in Fig. 8. Fig. 8(a) shows a group of particles with $E_p = 10^6$ V/m, $k_z = 27$ m^{-1}, and the remaining parameters given in Table II. The solid lines represent the perturbed azimuthal motion of individual particles, $l[\phi(t) - \omega_c t] = l[\phi_{00} + \phi_1(t)]$. The dashed lines represent the corresponding motion of the zeros of E_ϕ, with the positive part of the field initially between $-180°$ and $0°$. Bunching due to the negative mass effect can easily be seen. Trapping can also be seen as some particles do not cross the outer boundaries of the wave period, represented by the dashed lines which begin at $l\phi = -180°$ and $l\phi = +180°$. In Fig. 8(b) we plot, for this group, the net energy loss per particle of trapped and untrapped particles as well as the total energy change; the initial energy is 2.555 MeV. The average energy loss of the trapped particles is close to the total energy loss, and the trapped particle curve is a fairly good approximation of the total curve.

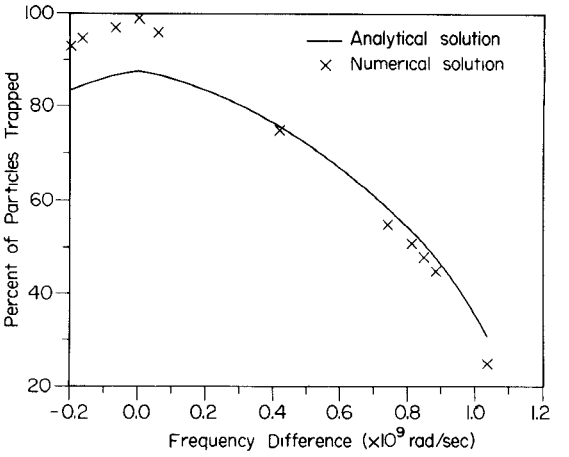

Fig. 7. Percentage of particles trapped versus distance from resonance from both the analytic trapped solution and the numerical solution.

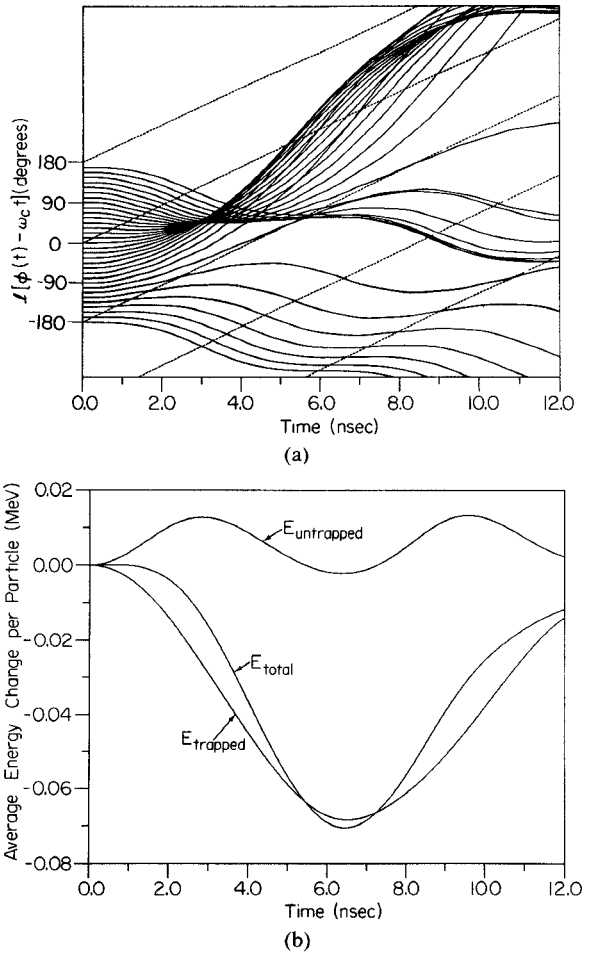

Fig. 8. (a) Group of particles at $k_z = 27$ m^{-1} and $E_p = 10^6$ V/m showing bunching and trapping. (b) Comparison of the contributions to total energy loss from the trapped particles and untrapped particles in (a).

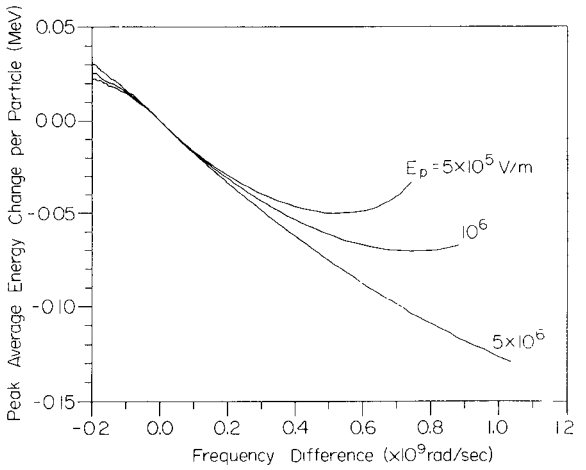

Fig. 9. Energy loss versus distance from resonance for different peak electric fields using the analytic trapped solutions.

In Fig. 9, peak average energy loss versus distance from resonance is shown. This plot, when combined with the plot showing the percentage of trapped particles, illuminates the interrelation between energy loss, location of the bunch in the wave, and number of trapped particles. For the base problem with $E_p = 10^6$ V/m, the optimum distance from resonance occurs at approximately 0.75×10^9 rad/s, which corresponds to $k_z = 27$ m^{-1}. At this point about 55 percent of the particles are trapped, and Fig. 8 shows that the bunch forms almost exactly at the peak of the azimuthal electric field. While these results apply to a particular set of parameters, they illustrate the importance of both the number of particles trapped and the average electric field "seen" by these trapped particles. Fig. 9, together with Fig. 7, shows that close to resonance it is the position of the bunch that limits the energy loss while far from resonance it is the percentage of trapped particles that limits energy loss.

From (26), (29), (30), and (31), the error produced by neglecting ϕ_2, which is also the error in using (19) to approximate ϕ_1, can be evaluated. The largest error occurs for the particles on the trapping border and is found to be about 13 percent. It is instructive, however, to see where this error manifests itself. Fig. 7 shows that, at resonance, the difference between the analytic and numerical solutions for the percentage of trapped particles is indeed about 13 percent, while away from resonance it is much less. This is because the error occurs in the equations of a_1. For particles close to the trapping border and away from resonance, a small difference in ϕ_{00} translates into a large difference in a_1; working backwards, a 13-percent error in a_1 becomes a smaller error for ϕ_{00}.

V. Summary and Conclusions

This paper contains a study of the single-particle motion in a TE_{71} cylindrical waveguide mode in a large-orbit gyrotron. The field amplitude is "small" and remains constant. The parameters which are varied in this study are the initial azimuthal position of the particle, ϕ_{00}, the axial wavenumber k_z, and the wave amplitude E_p. The axial wavenumber is important because it determines the frequency difference between the particles and the wave. The fixed parameters are close to those of the LOG experiment on the RBF at the University of Maryland.

By varying these parameters, two important characteristics of the particle motion can be observed. One is bunching due to the negative mass effect. This can be seen by uniformly distributing a group of particles within one azimuthal wave period. For a LOG this bunching is not only in phase but also in physical space. The other characteristic is trapping, which can be studied by varying k_z and/or E_p for a group of particles distributed in an azimuthal wave period.

Two different analytic solutions are developed. One is valid for untrapped particles, the other for trapped particles. These solutions indicate that first-order energy loss is due solely to the trapped particles. The trapped particle solutions can be used to estimate the number of trapped particles for a given k_z and E_p, and the minimum E_p for a given k_z at which trapping first occurs. The trapped solutions also accurately predict all of the trends associated with varying k_z and E_p. Both of the solutions give a good approximation to the numerical results in their respective regions of validity. Close to a tangential intersection between the waveguide curve and the beam line, the validity of the approximations used to obtain the trapped solutions improves, and the trapped solutions are more accurate than in the case of a general intersection. This fact is important because most gyrotrons are designed to operate at tangential intersection. There is a region in which $l\phi_1$ is a significant fraction of 2π even though the particles are not trapped. In this region neither analytic solution is a good approximation to the exact results; however, this group of particles is not important to energy loss.

Energy loss is a function of the number of trapped particles and the phase of the wave in which the bunch forms. Both of these are functions of k_z and E_p. For maximum energy loss, a large fraction of the particles must be trapped. In addition, bunch formation must occur well into the positive half of the azimuthal wave period. These two requirements, which oppose one another, balance to give an optimum k_z for a given E_p. The analytic trapped solutions can be used to find this optimum k_z for energy loss. While the equation for k_z is transcendental and involves a numerical integration over ϕ_{00}, its solution is found rapidly compared to a particle simulation.

Acknowledgment

Computer time was contributed by the Electrical Engineering Department. The authors would like to thank S. Swanekamp for his aid in generating some of the graphs.

References

[1] P. Sprangle, "Excitation of electromagnetic waves from a rotating annular relativistic e-beam," *J. Appl. Phys.*, vol. 47, pp. 2935–2940, 1976.

[2] W. W. Destler, H. Romero, C. D. Striffler, R L. Weiler, and W. Namkung, "Intense microwave generation from a non-neutral rotating e-layer," *J. Appl. Phys.*, vol. 52, pp. 2740–2749, 1981.

[3] W. Lawson and C. D. Striffler, "A general linear growth rate formula for large orbit, annular electron beams," *Phys. Fluids*, vol. 28, pp. 2868–2877, 1985.
[4] V. A. Flyagin, A. V. Gaponov, M. I. Petelin, and V. K. Yulpatov, "The gyrotron," *IEEE Trans. Microwave Theory Tech.*, vol. MTT-25, pp. 514–521, 1977.
[5] V. L. Granatstein, M. E. Read, and L. R. Barnett, *Measured Performance of Gyrotron Oscillators and Amplifiers* (Infrared and Millimeter Waves, vol. 5). New York: Academic Press, 1982, p. 267.
[6] R. S. Symons and H. R. Jory, *Cyclotron Resonance Devices*, (Advances in Electronics and Electron Physics, vol. 55). New York: Academic Press, 1981, pp. 1–75.
[7] L. E. Thode and R. N. Sudan, "Plasma heating by relativistic electron beams: I—Two-stream instability," *Phys. Fluids*, vol. 18, pp. 1552–1563, 1975.
[8] L. E. Thode, "Energy lost by a relativistic electron beam due to two-stream instability," *Phys. Fluids*, vol. 19, pp. 305–315, 1976.
[9] P. Sprangle and A. T. Drobot, "The linear and self-consistent nonlinear theory of the electron cyclotron maser instability," *IEEE Trans. Microwave Theory Tech.*, vol. MTT-25, pp. 528–544, 1977.
[10] J. L. Vomvoridis, "An efficient Doppler-shifted electron-cyclotron maser oscillator," *Int. J. Electron.*, vol. 53, pp. 555–571, 1982.
[11] P. Vitello, W. H. Miner, and A. T. Drobot, "Theory and numerical modeling of a compact low-field high-frequency gyrotron," *IEEE Trans. Microwave Theory Tech.*, vol. MTT-32, pp. 373–386, 1984.
[12] M. Abramowitz and I. A. Stegun, *Handbook of Mathematical Functions*. New York: Dover, 1954, p. 361.

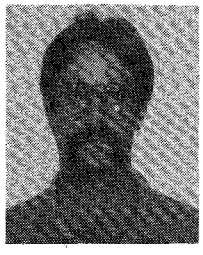

Hans P. Bluem attended UCLA and received the B.S. degree in electrical engineering in 1984. He received the M.S. in electrical engineering from the University of Maryland at College Park in 1986. Currently he is working on the Ph.D. degree at the University of Maryland, where he works with the Charged Particle Beam Group on fast-wave microwave tubes.

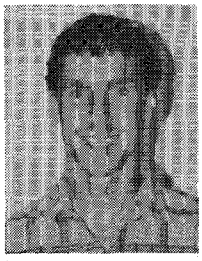

Peter E. Latham received the B.A. degree from the University of California at San Diego in 1977. He then went on to the University of California at Berkeley, where he received the M.A. in physics in 1979 and the Ph.D. in physics in 1986. Currently he is working on high-power microwave devices, including gyrotrons and free electron lasers, at the University of Maryland.

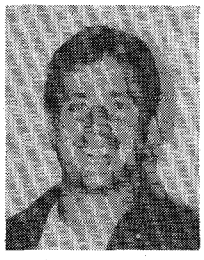

Wesley G. Lawson (S'84–M'85) was born in Akron, OH, in 1958. He received the B.S. degree in mathematics and the B.S., M.S., and Ph.D. degrees in electrical engineering from the University of Maryland. He worked four years on electronics at Harry Diamond Laboratories and has worked five years on microwave sources at the University of Maryland's Charged Particle Beam Laboratory.

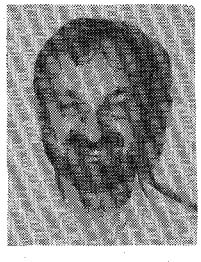

Charles D. Striffler (M'77) received the B.S. degree in science engineering and the M.S. and Ph.D. degrees in nuclear engineering from the University of Michigan in 1961, 1963, and 1972, respectively.

He was at Knolls Atomic Power Laboratory from 1965 to 1967, the Naval Research Laboratory from 1972 to 1975, and has been at the University of Maryland since 1974, where he is a Professor in the Electrical Engineering Department. His areas of research in the plasma physics field are high-power microwave generation in gyrotron devices, beam propagation and collective ion acceleration in intense relativistic electron beam systems, high-power short-pulse microwave propagation in the atmosphere, and energy recovery in large-orbit gyrotron devices.